D^3 Scaling Up Deepfake Detection by Learning from Discrepancy

Yongqi Yang[1⋆], Zhihao Qian[1⋆], Ye Zhu[2], and Yu Wu[1]

[1] Wuhan University, Wuhan Hubei 430072, China
[2] Princeton University, Princeton NJ 08544, USA

Abstract. The boom of Generative AI brings opportunities entangled with risks and concerns. In this work, we seek a step toward a universal deepfake detection system with better generalization and robustness, to accommodate the responsible deployment of diverse image generative models. We do so by first scaling up the existing detection task setup from the one-generator to multiple-generators in training, during which we disclose two challenges presented in prior methodological designs. Specifically, we reveal that the current methods tailored for training on one specific generator either struggle to learn comprehensive artifacts from multiple generators or tend to sacrifice their ability to identify fake images from seen generators (i.e., *In-Domain* performance) to exchange the generalization for unseen generators (i.e., *Out-Of-Domain* performance). To tackle the above challenges, we propose our **D**iscrepancy **D**eepfake **D**etector (**D^3**) framework, whose core idea is to learn the universal artifacts from multiple generators by introducing a parallel network branch that takes a distorted image as extra discrepancy signal to supplement its original counterpart. Extensive scaled-up experiments on the merged UFD and GenImage datasets with six detection models demonstrate the effectiveness of our framework, achieving 5.3% accuracy improvement in the OOD testing compared to the current SOTA methods while maintaining the ID performance.

1 Introduction

Recent advances in generative modeling have marked a new era of Generative AI, which is transforming society as it progresses from our research community into the real world. The widespread appeal of generative AI technologies among the general populace can be attributed to the significant achievements in scaling generative models—such as BigGAN [4], DALL·E [35], and StableDiffusion [36] — to unprecedented model sizes and leveraging expansive, open-world datasets. However, with these opportunities come inherent risks; these advancements also raise concerns about diverse aspects including data privacy, AI ethics, social fairness, and regulatory compliance [15]. Among these challenges, the risk of malicious use of synthetic data stands out as one of the particularly pressing issues that demand focused research attention.

⋆ Equal contribution.

Deepfake detection, which aims at discerning between real and generated fake images, acts as a crucial defense in responsibly deploying large generative models in the real world. The effectiveness of these detection systems largely depends on their generalization capability; ideally, they should reliably identify any synthesized image as fake, regardless of the generating source (i.e., the deep generative models from which they are generated). Accordingly, current deepfake detection methods [5; 10; 29; 32; 45; 46] usually follow a standard task setup for evaluating the performance, which involves training on images from one specific generator and testing on images from various unseen generators. As a natural step towards a universal deepfake detection foundation model, in this work, we propose to **scale up** this current setup from *"train-on-one and test-on-many"* to *"train-on-many and test-on-many"*, to accommodate the rapid development pace from the generative modeling side and better align with the real-world scenario.

However, in the process of scaling up existing deepfake detection models to multiple generators, we encounter **two challenges that have not yet been adequately addressed in prior literature,** limiting the generalization performance and robustness of an expanded detection system. *First*, we reveal that the existing methodology designs tailored for the *"train-on-one and test-on-many"* setup **struggle to learn the comprehensive and universal artifacts** when the fake images in training present different fingerprint patterns from more than one generator. For instance, one of the current SOTA detection models, DIRE from ICCV'23 [46], tends to learn the most obvious generator-specific artifacts (e.g., fingerprints of diffusion models [21; 42]) but overlooks the subtle but invariant common artifacts shared by other generative AI models (e.g., fingerprints from GAN-based generators [17]), leading to inferior testing performance on the images produced by unseen generators. As detailed in Sec. 4, our experimental results show that, when scaling up to 8 training generators and 12 unseen generators, DIRE [46] achieves 97.6% on in-domain (ID) testing, but performs significantly worse on the critical out-of-domain (OOD) testing with only 68.4% accuracy. *Second*, our empirical analysis further suggests that **prior methods tend to comprise the trade-off between training and testing performance**, by "underfitting" the ID training to barter for better OOD generalization ability in testing. As a concrete example, another SOTA detection method, UFD from CVPR'23 [32], achieves better generalization on OOD testing with an accuracy of 81.4% compared to DIRE [46]. However, the better OOD performance of UFD comes with the expense of the lower ID testing performance, resulting in only 86.6% on the ID accuracy.

To tackle the above challenges on the way of scaling up the deepfake detection methods to a universal system, we introduce our $\mathbf{D^3}$ framework, terminology from **D**iscrepancy **D**eepfake **D**etector, for an extended setup under the *"train-on-many and test-on-many"* scenario. The secret recipe of $\mathbf{D^3}$ lies within the core idea of **exploiting and learning the universal artifacts among various deep generators**, which intuitively facilitates the learning and improves the testing robustness. Specifically, unlike the existing methods [5; 32; 45] that feed the detection model only with either real or generated images, we adopt a two-

branch design to provide $\mathbf{D^3}$ with an extra corrupted image corresponding to its original counterpart, as illustrated in Fig. 1 and detailed in Sec. 3. The distorted image, which is obtained via operations such as patch shuffling, flipping, and rotation, deconstructs the unique fingerprint from a specific generator and serves as a discrepancy signal to supplement the original image. This unique methodological design encourages the proposed $\mathbf{D^3}$ framework to effectively capture the invariant artifacts from the image pair. We further improve the robustness and generalization ability of our $\mathbf{D^3}$ by extracting the image features from the CLIP encoder [34], and enhance their interactions via self-attention layers before making the final prediction.

We perform extensive experiments by gradually scaling up six deepfake detection methods (including [5; 29; 32; 45; 46] and our proposed $\mathbf{D^3}$) from conventional setup to 8 training generators and 12 testing unseen generators, on the UniversalFakeDetect (UFD) [32] and the GenImage [52] datasets. Each detection model is trained till convergence to ensure a fair comparison. Our comprehensive experiments and analysis not only explicitly disclose the two previously mentioned issues, but also demonstrate the effectiveness of our proposed $\mathbf{D^3}$ by outperforming SOTA methods with 5.3% on the OOD testing mean accuracy.

In summary, our work has the following contributions:

- We propose to scale up the current deepfake detection setup from *one-generator* to *multiple-generators* in training to accommodate the fast development pace from the generative modeling side and disclose two factors in the existing methods that limit the generalization ability and robustness in this extended detection scenario.
- We introduce our **D**iscrepancy **D**eepfake **D**etector ($\mathbf{D^3}$) framework to address the above challenges, whose core idea is to learn the general artifacts among multiple generators with an extra distorted image as the discrepancy signal via a parallel network branch.
- We perform extensive experiments, by gradually scaling up the current setup to 8 generators, and achieve 5.3% improvement in the OOD testing performance compared to SOTA methods, while maintaining the ID performance.

2 Related Work

With the swift advancement of generative models [13; 18; 21; 27; 36; 39; 43] and customization methods [16; 26; 38; 47; 49; 53], synthesized images are becoming increasingly realistic, making it challenging for the human eye to differentiate between real and fake images. To counter potential malicious usage, a considerable amount of research has been devoted to detecting generated images, yielding impressive identification accuracy.

2.1 Artifact-based Detection Methods

These methods explicitly extract artifacts in generated images in a preprocessing way. They usually directly estimate the artifacts [22; 50], compute the residual

noise between the original image and its reconstructed one [29; 30; 46], or calculate gradients [44]. [30] was the first to reveal that GANs leave specific fingerprints on the generated images. This was achieved by extracting the noise residual through an appropriate denoising filter, demonstrating its potential for forensic analysis. [50] proposed a GAN simulator to emulate the artifacts produced by the common pipeline shared by several popular GAN models. [22] proposed a fingerprint generator to cover the fingerprints of various GAN models to achieve generalized detection ability and avoid data dependency. LNP [29] pretrain a reconstruction network with only real images to extract the Learned Noise Patterns (LNP), which can explicitly embody artifacts. DIRE [46] used the prior from a pre-trained diffusion model to determine whether an image is within the distribution of fake images. This was achieved by computing the Diffusion Reconstruction Error (DIRE). [44] employed a pre-trained CNN model to extract the gradients of target images as the representation of artifacts.

However, their artifact extraction and simulation capabilities are limited by the prior knowledge derived solely from particular models. Therefore, they can not deal with samples generated by unfamiliar generators, making it difficult to be universally applied to real-world applications.

2.2 Learning-based Detection Methods

This type of method considers directly learning the artifacts from raw images. They aim to design a better network to extract more discriminative features. CNNDet [45] directly trained ResNet50 as the classifier on their proposed semantic-aligned dataset, containing fake images generated by ProGAN. Their methods exhibited strong generalization capabilities to other CNN-based generative models. Patchfor [5] used a fully convolutional patch-based classifier, emphasizing local patches over global structure. [19] modified the ResNet50 network with two fewer down-sampling layers to improve the detection performance. However, the learning-based methods directly train the entire network to learn the presence or absence of actual artifact patterns. They often overlook features inherent to real images, which can lead to overfitting and poor generalization.

2.3 CLIP-based Detection Methods

To mitigate the shortcomings of the learning-based methods, this type of method leverages the frozen feature space of CLIP to extract more generalizable features. UFD [32] first highlighted that a feature space not explicitly learned for generated image detection is more effective due to its unbiased decision boundaries. Consequently, they performed detection in the pre-trained CLIP feature space using linear probing or nearest neighbor methods, demonstrating impressive generalization performance on unseen generated images. Taking a further step in this direction, [10] trained SVMs with the features from the penultimate layer and achieved commendable performance despite a limited amount of well-organized training data. Likewise, [41] additionally utilized the text encoder of

the pre-trained CLIP model to exploit the prompt information by concatenating the encoded image embeddings and text embeddings together as features. However, these CLIP-based methods employ only one linear classifier to distinguish between real and fake features of images. Therefore, when applied to a larger multi-generator dataset, the simple classifier struggles to effectively fit the ID data, which further impacts OOD performance. In this work, we further enhance the fitting and generalization ability of CLIP-based detectors on multi-generator datasets. We propose to learn more stable and invariant artifacts by comparing images before and after corruption. Our approach facilitates a better understanding of the universal differences between real and fake images.

3 Scaling Up Deepfake Detection

We formulate the extended *"train-on-many and test-on-many"* setup in Sec. 3.1, and identify the key challenges for a generalized and robust detection system in Sec. 3.2. Sec. 3.3 introduces our proposed $\mathbf{D^3}$ method.

3.1 Problem Formulation

Formally, given a generator set $\mathcal{G}$ composed of N different types of generators, $\mathcal{G} = \{G_i\}_1^N$, $\mathcal{R}_i = \{r_1^{(i)}, r_2^{(i)}, \dots, r_{N_i}^{(i)}\}$ and $\mathcal{F}_i = \{f_1^{(i)}, f_2^{(i)}, \dots, f_{N_i}^{(i)}\}$ denote the real and fake samples of $\mathcal{G}_i$, where N_i is the number of samples in each class. Our goal is to correctly distinguish between real and fake when given any image from the overall dataset, $\mathcal{D} = \{\{\mathcal{R}_i\}_1^N \cup \{\mathcal{F}_i\}_1^N\}$. The existing detection task setup involves training on one of the generators G_i. In terms of evaluation, they regard the seen generator G_i as the ID generator and the other unseen generators $\{G_j\}_{j \neq i}$ as the OOD generators. This setup implies learning to detect universal artifacts from only one specific kind of artifact, which is hard and unnecessary. This impractical setup may mislead the research community because the generalization performance is unstable and would highly depend on the choice of the training generator. For example, the OOD performances of UFD [32] would drop significantly from 87.6% to 58.9% when switching the training from the ProGAN [23] to Midjourney [2] in this scheme.

Therefore, we propose to step out of the "train-on-one and test-on-many" task setup and leverage a new *"train-on-many and test-on-many"* evaluation scheme. More specifically, we add more generators into the current dataset and train on a subset composed of k ($k < N$) generators, denoted by $\mathcal{G}_s = \{G_{s_i}\}_1^k (s_i \in \{1, 2, \dots, N\})$. In this way, we regard the k generators in $\mathcal{G}_s$ as the ID generators and the other $N-k$ generators as the OOD generators. In practice, we merge two large-scale existing deepfake detection datasets, i.e., the UFD dataset [32] and GenImage dataset [52]. Finally, there are in total 20 state-of-the-art generators available in the scale-up setup. Considering the diversity, we regard all the 8 generators used in different previous works, including 2 GANs methods like ProGAN [23], and 6 DMs like ADM [13]. The rest 12 generators (including both GANs and DMs) are used as the OOD set.

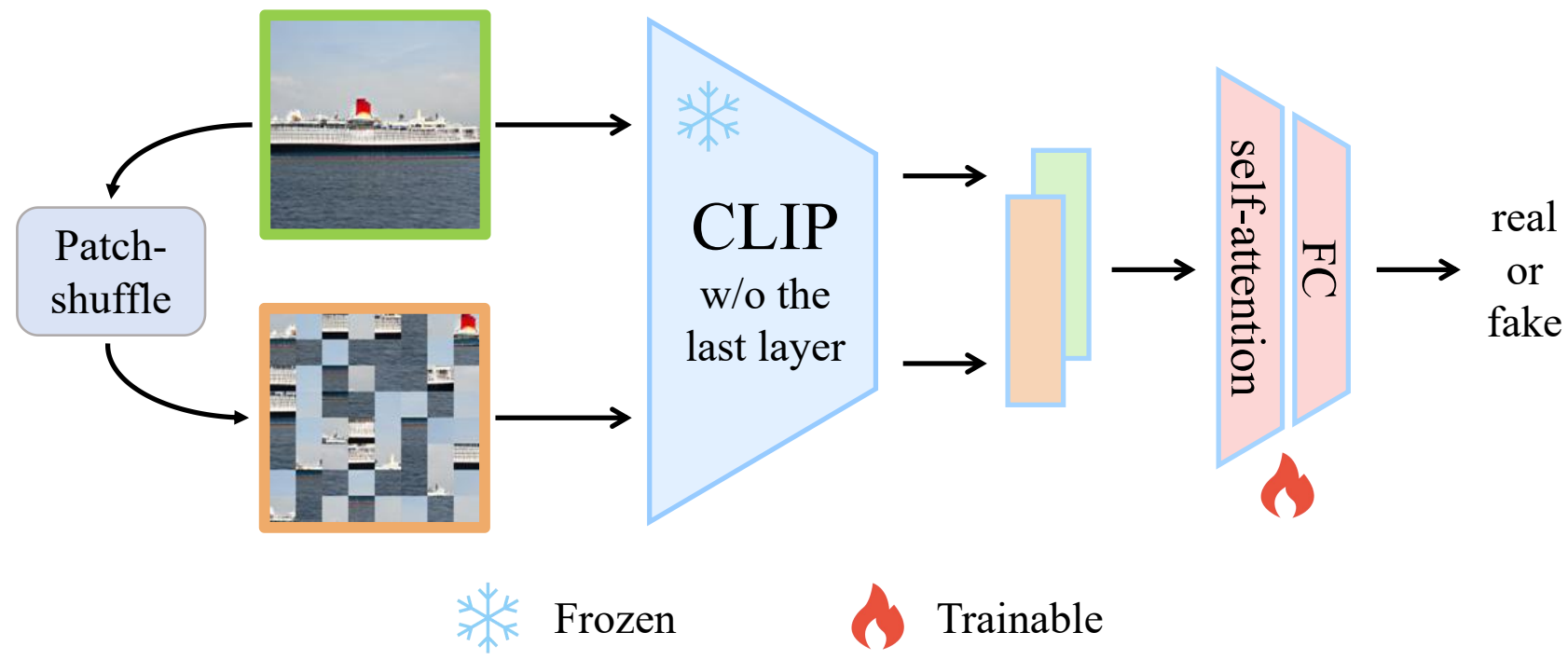

Fig. 1: The overall framework of our Discrepancy Deepfake Detector (D^3). The original image and its patch-shuffled variant are inputted into the pre-trained CLIP model [34] to obtain two features. We then utilize the self-attention module to encourage the learning of shared artifacts between the features. Finally, we use a single-layer linear classifier to get the final prediction.

3.2 Challenges in the Scaled-up Setup

Based on the scaled-up setup, we gradually add the generators into the training pool in different random orders to evaluate the existing works. As the number of generators increased from one to eight, we found existing methodology designs tailored for the previous setup could not learn universal artifacts. For example, one of the state-of-the-art works UFD [32] from CVPR'23 even decreases significantly in terms of ID testing accuracy as more generators are used for training (Fig. 2), demonstrating the underfitting issue. While another state-of-the-art work DIRE [46] from ICCV'23 shows extremely good ID performance (97.6%), it suffers from the generalization issue that the OOD testing accuracy is not promising (68.4%), despite it has already seen eight advanced generators covering typical GANs and DMs. These results suggest existing models could not find the invariant artifacts that are universal in multiple generators. The main reason might be the universal data patterns we wish the model to learn are coupled with or hidden by semantics. It inspires us to go deeper to learn universal artifacts rather than the superficial and generator-specific artifacts that can be directly seen on the deepfake images.

3.3 D^3: Deepfake Dectection by Learning from Discrepancy

Overall Pipeline. Our proposed framework for generative image detection is depicted in Fig. 1. Overall, the original image and its patch-shuffled counterpart are input into the pre-trained CLIP [34] model to obtain visual features. A self-attention layer is then used to promote learning from the discrepancy between the two features. Finally, a linear classifier is employed to predict real or fake labels. The design of each module will be discussed in the following.

Visual Backbone. Directly learning on the deepfake detection data without pretraining can lead to overfitting on the training generators, resulting in poor

generalization to OOD generators [9; 52]. To mitigate this, we follow previous work [10; 32] and adopt the pre-trained CLIP:ViT-L/14 as our feature extractor. More specifically, we extract features from the penultimate layer of the pre-trained CLIP model, which keeps more detailed visual clues of the input.

Dual-Path Discrepancy Learning. To encourage the model to find deeper robust artifacts, we propose to introduce an additional branch that takes a corrupted image as input. Given an original image x_o from the dataset $\mathcal{D}_s = \{\{\mathcal{R}_i\}_1^k \cup \{\mathcal{F}_i\}_1^k\}$, corresponding to the subset $\mathcal{G}_s$. In the new branch, we divide the input image x_o into patches, and then randomly shuffle them to form a new image, where the superficial artifacts will be destroyed to avoid the model simply learning a generator-specific shortcut. After that, we input the corrupted data to the same visual backbone to extract features,

$$e_o = \texttt{CLIP}^*(\texttt{AUG}(x_o)), e_s = \texttt{CLIP}^*(\texttt{PatchShuffle}(\texttt{AUG}(x_o))), \tag{1}$$

where e_o and e_s are the visual embeddings of the respective images, $\texttt{CLIP}^*$ denotes the extraction of the penultimate feature using the pre-trained CLIP model, `PatchShuffle` is the patch-shuffling operation, and `AUG` represents the common data augmentation method used in the previous work [45].

Self-Attention Invariance Extraction. Having obtained two features, e_o and e_s, from the original and patch-shuffled images respectively, we stack the two features together, $e = [e_o, e_s]$. The correlation between e_o and e_s is crucial for detecting fake images. To this end, we employ a self-attention layer on the stacked feature e to extract the shared artifact feature E by learning the associations between the features. In this way, we force the model to learn from the discrepancy between the original image and its patch-shuffled image. In experiments, we found the more distinct between the original image and the corrupted image, the better the deepfake detection performance the model can get.

Loss Function. Based on the fused feature E, we employ a single fully connected layer, denoted as $\Phi(\cdot)$, to compute the classification logits. We then train the model using the binary cross entropy loss by,

$$\mathcal{L} = -\frac{1}{N_B}\sum_{i=1}^{N_B}(y_i \log(\Phi(E)) + (1 - y_i)\log(1 - \Phi(E))), \tag{2}$$

where N_B is the batch size, and y_i is the label of the i-th input sample. Note that our visual backbone is frozen, thus the learnable parameters are only self-attention and the classification layer.

4 Experiments

4.1 Scaled-Up Datasets

To evaluate the effectiveness of our proposed method, we conducted experiments on the UniversalFakeDetect dataset [32] and the GenImage dataset [52]. Notably, we scale up the experimental data by merging the two datasets together.

The **UniversalFakeDetect** (abbreviated to "**UFD**") dataset contains 720k images in its training set, including 360k real images (drew from LSUN [48], LAION [40] and ImageNet [12]) and 360k fake images generated by different generators including GANs like ProGAN [23], CycleGAN [51], BigGAN [4], StyleGAN [24], GauGAN [33], StarGAN [8], Deepfakes [37], SITD [6], SAN [11], CRN [7] and IMLE [28], and diffusion models like Guided Diffusion [13], LDM [36], GLIDE [31] and DALL·E [35].

The **GenImage** dataset comprises 2,681,167 images, segregated into 1,331,167 real (drawn from ImageNet) and 1,350,000 fake images, with 50k images left for testing in each generator type. Fake images in this dataset are generated by 8 generators, including 1 GAN (BigGAN [4]) and 7 diffusion models (Stable Diffusion V1.4 [36], Stable Diffusion V1.5 [36], GLIDE [31], VQDM [20], Wukong [3], ADM [13] and Midjourney [2]).

In our new setup, we merge the two datasets into one and regard generators with the same architecture but different parameters (*e.g.* SD v1.4 and SD v1.5) as the same type. To this end, we eliminate SD v1.5 from the merged training set and remain SD v1.4. Besides, we also make sure each generator has an equal number of samples to avoid imbalanced data. Finally, there are a total of 20 generators available in the scale-up setup, 8 in the training set (2 GANs and 6 Diffusions) and 12 in the OOD set. Compared with the former setup, we have scaled up both the number of generators and the volume of samples within the training set. Besides, we further split 10% samples in the testing set of our merged dataset per generator as the validation and the rest as the testing set.

4.2 Implementation Details

In our experiments, we employ the CLIP: VIT-L/14 model pre-trained on a large dataset WebImageText as the backbone to extract patch tokens. We adopt its penultimate feature before dimensionality reduction for better representation. With the backbone frozen, the whole network is trained on a single NVIDIA RTX 4090 with a batch size of 128 within 5 epochs. We apply the Adam optimizer with an initial learning rate of 0.0001 and a weight decay of 0. During training, all images are resized to 256x256 resolution and then randomly cropped to 224x224 resolution. We adopted the data augmentation scheme the same as the works [32; 45], involving Gaussian blur and JPEG compression. Specifically, the *quality* of JPEG compression randomly ranges from 30 to 100, the *sigma* of Gaussian blur randomly ranges from 0 to 3, and their occurrence probabilities are set to 0.5. During validation and testing, we directly resize the image to the size of 224x224, without any augmentation.

4.3 Experimental Setup

In this subsection, we provide a detailed illustration of our experimental setup, including the implementation of baselines and evaluation metrics.

Implementation of Baselines. In terms of baselines, we re-implement the comparison methods according to their official codes under our problem settings for fairness. The baselines include CNNDet [45], Patchfor [5], LNP [29], DIRE [46], and UFD [32]. Detailedly, CNNDet finetunes a pre-trained ResNet50 as a classifier and we use the ResNet50 version with default parameters. Patchfor finetunes the truncated ResNet or Xception as the classifier at the patch level and we choose their Xception version. LNP pre-trains a reconstruction model with only real images to extract noise patterns and then finetunes the pre-trained ResNet50 with spatial and spectrum information. We use their pre-trained reconstruction model to preprocess all the images and finetune the ResNet50 in the default way. DIRE first computes the diffusion reconstruction error of all images and trains a ResNet50 on them. We use their 256x256 unconditional DMs to preprocess all the images and also finetune the ResNet50 in the default way. UFD extracts the features with a frozen CLIP model and classifies them by nearest neighbors or linear probing. We select their linear probing version with the CLIP: VIT-L/14 as the backbone. In our experiments, all methods are re-implemented with their default settings in our new setup, and the optimal checkpoint is selected based on the performance on the validation set to ensure a fair comparison.

Evaluation Metrics. We employ mean classification accuracy (Mean acc.) and average precision (AP) to evaluate the performance of detectors. When calculating overall mean accuracy, we first average the accuracy of different variants of the same generator (*e.g.* SD1.4 and SD1.5). Then, we average all the accuracy scores across different generators. Note that we use a fixed threshold of 0.5 when calculating the accuracy score for each detector.

AP quantifies the separability between fake and real images, neglecting the specific threshold consideration. Previous literature [29; 32; 45; 46] typically uses mAP to represent the overall AP score, where they calculate AP for each generator independently and average the AP scores. However, the direct average of AP disregards the substantial variance in the optimal thresholds, or boundaries, between real and fake images from different generators. In practice, it is infeasible for users to set different real/fake thresholds for unseen generators. Therefore, we propose to calculate a global AP rather than mAP, which shares the same standards among all testing generators.

We first resample generators with the same architecture based on the maximum number of samples among them and merge them as one. Then, we similarly resample different types of generators to ensure the entire test set is evenly distributed. Finally, we calculate the average precision (AP) of different merged sets to represent the overall AP. For instance, in terms of ID AP, we merge the results of all ID generators to compute an overall ID AP. This approach ensures a balanced evaluation across different generators, providing a more accurate measure of the detector's performance.

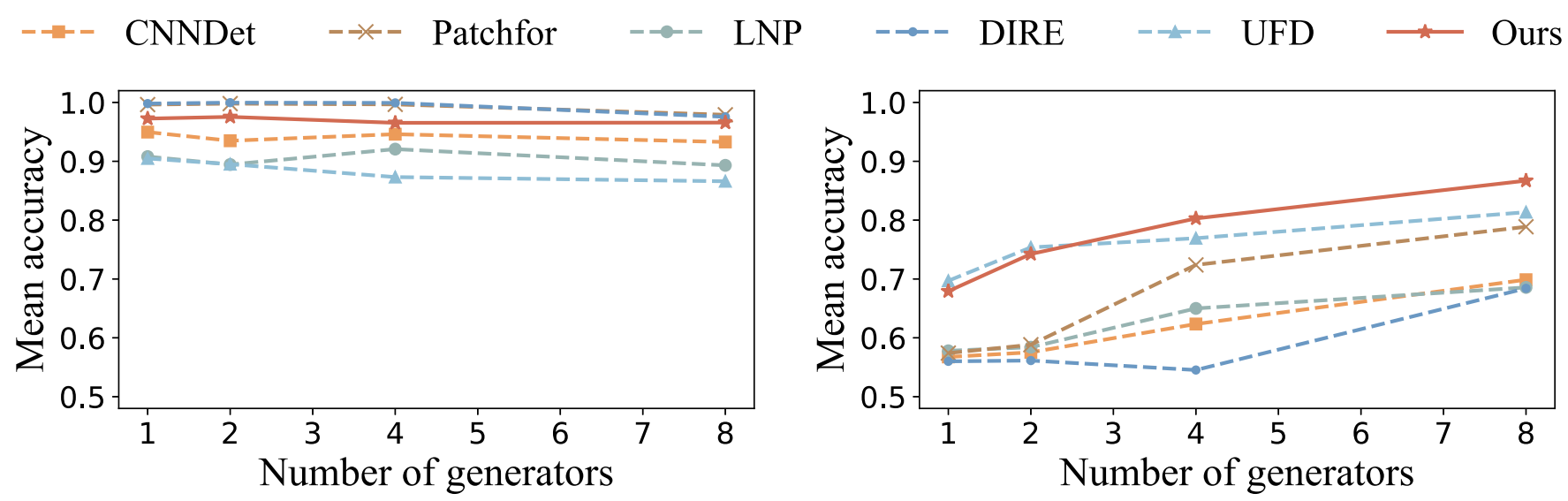

(a) In-domain (b) Out-of-domain

Fig. 2: Mean accuracy of training on scaled-up datasets on the testing set. We design an experiment to show the performance of different methods when gradually adding generators into the training pool. To avoid occasionality, we add the generator in three distinct random orders and average the corresponding test results. (a) "In-domain" means 1 shared training generator (*the first generator in any given order*). (b) "Out-of-domain" means 12 shared OOD generators.

4.4 Scaling Up the Training Data

In this section, we conduct experiments to show how the models perform as the generators gradually scale up in Fig. 2. We re-train the detectors on the training set with *{1, 2, 4, 8}* generators. To mitigate any potential bias, we add the generator in three distinct random orders and average the corresponding test results. To make all the curves comparable (in both horizontal and vertical), all detectors are evaluated on the same ID and OOD test sets, thus the curves are comparable in both horizontal and vertical and we can observe how a model baheves as the number of training generators grows. Note that only the first generator is commonly shared when gradually adding training generators from one to eight, we thus test all models only on this generator for the ID evaluation. For the OOD evaluation, we use the 12 common unseen generators for all models.

According to Fig. 2, as the number of generators increases, our method shows a slight fluctuation in ID performance and exhibits the highest performance and stable upward trend in OOD generalization. CNNDet [45] and Patchfor [5] show excellent ID fitting ability, but their OOD performances are inferior to the other works. It is worth mentioning that Patchfor to some extent alleviates the over-fitting issue by focusing on artifacts of local patches instead of the high-level features. Reconstruction-based methods like LNP and DIRE heavily rely on their pre-trained reconstruction model, which could result in poor generalization to unfamiliar domains. Moreover, the CLIP-based method UFD exhibits superior OOD performance when there are few generators and maintains a rising trend as the training set scales up. However, its ID performance continues to decline, which indicates a limitation in its representative capacity. In sum, these findings collectively demonstrate that our method effectively improves the distinguishability and generalizability of features by patch-shuffling and artifact invariance learning from the introduced discrepancy, resulting in stable and outstanding performance of ID fitting and OOD generalization.

Table 1: Comparisons to the SOTAs in mean accuracy (Mean acc.) and average precision (AP) on the testing set. "In-domain" includes 8 types of generators seen during training, "Out-of-domain" includes 12 types of generators, and "Total" includes all of them. Bold represents the best within the same metric. Our method achieves the best OOD and overall performance. A more detailed version of the result can be found in the Appendix D.

Methods	Pub.	Testing					
		In-domain		Out-of-domain		Total	
		Mean acc.	AP	Mean acc.	AP	Mean acc.	AP
CNNDet	CVPR20	0.933	0.906	0.699	0.679	0.792	0.770
Patchfor	ECCV20	**0.979**	**0.997**	0.789	0.880	0.865	0.942
LNP	ECCV22	0.881	0.902	0.719	0.797	0.784	0.823
DIRE	ICCV23	0.976	0.994	0.684	0.726	0.801	0.862
UFD	CVPR23	0.866	0.950	0.814	0.927	0.835	0.935
Ours	-	0.966	0.995	**0.867**	**0.943**	**0.907**	**0.968**

4.5 Comparison with the State-of-the-Art Methods

We compare our method with other state-of-the-art methods in the scale-up setup and report evaluation of their ID and OOD performance on the testing set. Tab. 1 reports the results on the testing set, where "In-domain" includes 8 types of generators, and "Out-of-domain" includes 12 types of generators, and "Total" includes all of them. A more detailed version of the result can be found in the Appendix D.

The experimental results exhibit the strengths and weaknesses of each method. CNNDet overfits data from familiar generators and performs poorly on data from unseen generators, consistent with the findings about ResNet in the paper [52]. Patchfor achieves the best ID mean accuracy and AP. However, its subpar OOD performance suggests that directly learning the specific local artifact patterns may also lead to a higher potential for overfitting. LNP exhibits poor performance in both ID and OOD fitting. DIRE demonstrates superior ID performance, surpassed only by Patchfor. However, it lacks generalization capabilities with OOD generators due to its tailored design for DMs. UFD's performance is second only to our method, but its ID performance is subpar.

In comparison, our method achieves the highest overall mean accuracy of 90.7% and AP of 96.8%, exceeding the second-best method, Patchfor, in overall mean accuracy by 4.2% and AP by 2.6%. Although our method marginally trails Patchfor in terms of ID accuracy and AP, it exhibits a more balanced and consistent overall performance. Furthermore, our method greatly outperforms UFD, which also leverages the pre-training CLIP, in ID mean accuracy by 10% and OOD mean accuracy by 5.3%. This underscores that our method further exploits the potential of CLIP-based feature representation ability by learning from the discrepancy of the shared artifact in the original image and its patch-shuffled variant.

Robustness Evaluation. We evaluate the robustness of all methods to align more closely with their practical effectiveness in real-world applications. Given

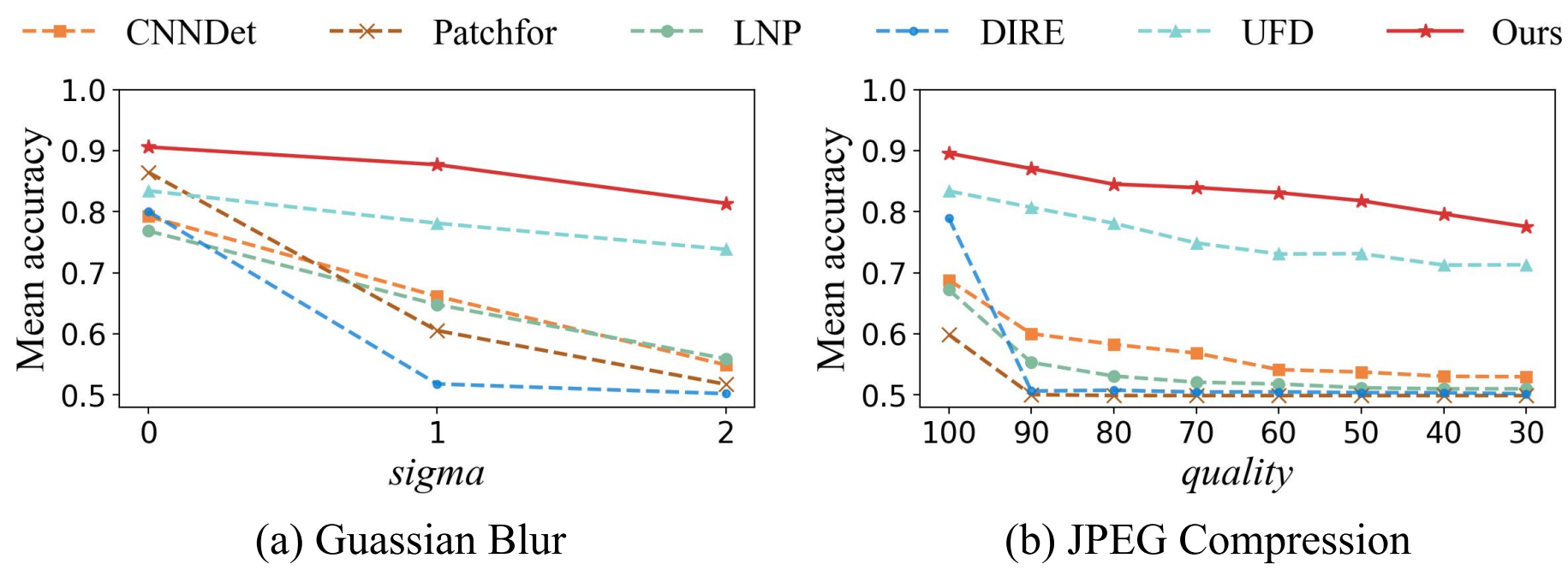

Fig. 3: Total mean accuracy results of robustness to post-processing operations on the testing set. We conducted experiments on Gaussian blurring ranging from 0 to 2 and JPEG compression ranging from 30 to 100 to verify the robustness of different methods to post-procession operations.

the potential for real-world images to undergo various degradations, ensuring the robustness of detectors against unseen perturbations becomes another vital aspect of evaluating their performance. A detector that can resist various perturbations and attacks has higher potential and value for practical application. Therefore, we evaluate all methods on two post-processing operations, Gaussian blurring (*sigma*: 0-2) and JPEG compression (*quality*: 30-100). Fig. 3 presents the results of our comparison with the other methods, demonstrating that our method exhibits the best robustness with a large margin with the other methods. Note that except for Patchfor and DIRE, all the other methods employ an augmentation strategy involving random Gaussian blurring and JPEG compression during training to enhance robustness. Despite this, we can observe that only our method and UFD exhibit general robustness, even to extremely heavy degradations. In addition, from the perspective of accuracy and the decay rate, our method shows obvious advantages compared to UFD. Discrepancy learning between the original image and its patch-shuffled one can to some extent offset the impact of these disturbances due to its concentration on more stable and invariant artifacts instead of specific artifact patterns.

4.6 Exploration of Different Disruptions

In this subsection, we investigate how different levels of disruptions influence model performance. We conduct experiments by only replacing the patch-shuffling operation with other disruption operations in our framework. These operations include horizontal flipping, vertical flipping, and random rotating (rotating an image with random degrees from 0° to 180°).

The experimental results are shown in Table 2, showing that disrupted feature helps in promoting the model performance, with the effectiveness of patch-shuffling, random rotating, vertical flipping, and horizontal flipping diminishing in sequence. The two-branch model with the **horizontal flipping** doesn't show superior to the one-branch baseline, because the horizontally-flipped image could not provide any discrepancy and its features are just the same as the original

Table 2: Experimental results of different disruptions on the validation set. We showed how different transformations influence model performance.

Augmentations	Validataion					
	In-domain		Out-of-domain		Total	
	Mean acc.	AP	Mean acc.	AP	Mean acc.	AP
Horizontal flipping	0.887	0.964	0.819	0.934	0.846	0.945
Vertical flipping	0.934	0.986	0.854	**0.937**	0.886	0.959
Random rotation	0.954	0.991	0.854	0.928	0.891	0.958
Patch shuffling	**0.972**	**0.995**	**0.874**	0.931	**0.913**	**0.962**

image for most existing vision models. Comparatively, **vertical flipping** has provided corruptions to the vision backbones to some degree since most vision models could not well recognize the image after vertical flipping. Thus the discrepancy helps the model learn better artifacts, leading to an overall performance boost of 4% on mean accuracy compared to the horizontal flipping. In addition, **random rotation** randomly changes the angle of images, introducing a slightly stronger semantic corruption on image semantics than the fixed 180° angle of vertical flipping, and thus has a slightly better overall performance. In comparison to the three operations, the **patch-shuffling** operation disrupts the image more completely, leading to the maximum discrepancy between the two branches. Thus it achieves the best performance. The comparison between different transformations clearly illustrates that the discrepancy between the original images and corrupted images helps the detector to learn more universal artifacts. The stronger semantic corruption the operation causes, the better the model performs.

4.7 Ablation Studies

In this subsection, we break down our framework into several key modules and explore the role of each module through ablation experiments. The ablation experimental results are shown in Table 3, where a tick represents the adoption of this module and the emptiness of Branch2 means using only one branch. The experiments have been numbered with groups for the following reference.

Patch-shuffling operation. A comparison between Group 2 and Group 4 reveals that the integration of the original image and the patch-shuffled image results in a substantial performance enhancement under the "SA"+"FC" classifier. This is evidenced by an increase of 7.8% in ID mean accuracy, 4% in OOD mean accuracy, and 5.5% in total mean accuracy. This effectively substantiates that combining the information from the original image and its patch-shuffled one can enhance the overall performance.

Discrepancy between Branches. Compared to Group 4, both Group 5 and Group 6 show an inferior performance, due to the absence of discrepancy features between two images of the same type. According to the table, Group 5 and Group 6 are 6.0% and 13.3% lower than group 4 in average mean accuracy, respectively. This further demonstrates that different inputs can provide different information, and assist the model to learn more universal artifacts.

Table 3: Results of ablation study on the validation set. We break down our framework into several key modules and explore the importance of each module through ablation experiments. The checkmark represents the adoption of the corresponding module. The emptiness of Branch 2 means using only one feature.

Group	Branch1	Branch2	CLIP	SA	FC	Validataion					
						In-domain		Out-of-domain		Average	
						Mean acc.	AP	Mean acc.	AP	Mean acc.	AP
1	Original	-	✓		✓	0.889	0.965	0.823	0.937	0.850	0.947
2	Original	-	✓	✓	✓	0.894	0.965	0.834	0.936	0.858	0.947
3	Original	Shuffled	✓		✓	0.918	0.977	0.835	**0.938**	0.868	0.954
4	Original	Shuffled	✓	✓	✓	**0.972**	**0.995**	**0.874**	0.931	**0.913**	**0.962**
5	Original	Original	✓	✓	✓	0.889	0.964	0.829	0.935	0.853	0.946
6	Shuffled	Shuffled	✓	✓	✓	0.841	0.914	0.738	0.800	0.780	0.849

Self-Attention Layer. Comparing Group 1 with Group 2, adding a self-attention layer to the single original feature only slightly improves the performance by approximately 1 point. However, comparing Group 3 with Group 4, adding a self-attention layer to two different features markedly enhances the performance with an increase of 5.5% in ID mean accuracy and 3.9% in OOD mean accuracy. This suggests that appropriately learning the connections between the shared artifacts in the original image and its patch-shuffled one, rather than merely enhancing the features, is another key to the success of our method.

In conclusion, each module is dispensable. The impact of any individual module may not be substantial, but their collective integration significantly enhances the performance. These findings provide robust evidence in support of our proposition that invariance-learning from discrepancy is beneficial for universal deepfake detection in a scaled-up scenario.

5 Conclusion and Discussion

Conclusion. In this paper, we propose a novel evaluation setup *"train-on-one and test-on-many"*, aimed at advancing the development of a universal deepfake detection system. To tackle the challenges in the new setup, we introduce our **D**iscrepancy **D**eepfake **D**etector (**D^3**) to learn the universal artifacts from multiple generators. We achieve this by introducing a parallel network branch that takes a distorted image as an extra discrepancy signal to supplement its original counterpart. Extensive experiments demonstrate the effectiveness of our framework, achieving 5.3% accuracy improvement in the OOD testing compared to the current SOTA methods and maintaining excellent ID performance.

Limitations. The parallel design of **D^3** requires running the CLIP twice to obtain two different features from one image, which doubles the computation cost compared with UFD. Moreover, our proposed setup demands a large-scale and comprehensive real-world dataset, while the merged dataset in our research may not fully meet this criterion in the future. Collecting such a high-quality generated image detection dataset may be expensive, however, it is not infeasible given the fast-increasing research scale in the community.

Bibliography

[1] http://www.whichfaceisreal.com/ (2019)
[2] https://www.midjourney.com/home/ (2022)
[3] https://xihe.mindspore.cn/modelzoo/wukong (2022)
[4] Brock, A., Donahue, J., Simonyan, K.: Large scale gan training for high fidelity natural image synthesis. ICLR (2019)
[5] Chai, L., Bau, D., Lim, S.N., Isola, P.: What makes fake images detectable? understanding properties that generalize. In: ECCV (2020)
[6] Chen, C., Chen, Q., Xu, J., Koltun, V.: Learning to see in the dark. In: CVPR (2018)
[7] Chen, Q., Koltun, V.: Photographic image synthesis with cascaded refinement networks. In: ICCV (2017)
[8] Choi, Y., Choi, M., Kim, M., Ha, J.W., Kim, S., Choo, J.: Stargan: Unified generative adversarial networks for multi-domain image-to-image translation. In: CVPR (2018)
[9] Corvi, R., Cozzolino, D., Zingarini, G., Poggi, G., Nagano, K., Verdoliva, L.: On the detection of synthetic images generated by diffusion models. In: ICASSP (2023)
[10] Cozzolino, D., Poggi, G., Corvi, R., Nießner, M., Verdoliva, L.: Raising the bar of ai-generated image detection with clip. arXiv (2023)
[11] Dai, T., Cai, J., Zhang, Y., Xia, S.T., Zhang, L.: Second-order attention network for single image super-resolution. In: CVPR (2019)
[12] Deng, J., Dong, W., Socher, R., Li, L.J., Li, K., Fei-Fei, L.: Imagenet: A large-scale hierarchical image database. In: CVPR (2009)
[13] Dhariwal, P., Nichol, A.: Diffusion models beat gans on image synthesis. NeurIPS (2021)
[14] Dosovitskiy, A., Beyer, L., Kolesnikov, A., Weissenborn, D., Zhai, X., Unterthiner, T., Dehghani, M., Minderer, M., Heigold, G., Gelly, S., et al.: An image is worth 16x16 words: Transformers for image recognition at scale. ICLR (2021)
[15] Epstein, Z., Hertzmann, A., of Human Creativity, I., Akten, M., Farid, H., Fjeld, J., Frank, M.R., Groh, M., Herman, L., Leach, N., et al.: Art and the science of generative ai. Science (2023)
[16] Gal, R., Alaluf, Y., Atzmon, Y., Patashnik, O., Bermano, A.H., Chechik, G., Cohen-Or, D.: An image is worth one word: Personalizing text-to-image generation using textual inversion. ICLR (2023)
[17] Goodfellow, I., Pouget-Abadie, J., Mirza, M., Xu, B., Warde-Farley, D., Ozair, S., Courville, A., Bengio, Y.: Generative adversarial nets. NIPS **27** (2014)
[18] Goodfellow, I., Pouget-Abadie, J., Mirza, M., Xu, B., Warde-Farley, D., Ozair, S., Courville, A., Bengio, Y.: Generative adversarial nets. NeurIPS (2014)

[19] Gragnaniello, D., Cozzolino, D., Marra, F., Poggi, G., Verdoliva, L.: Are gan generated images easy to detect? a critical analysis of the state-of-the-art. In: ICME (2021)

[20] Gu, S., Chen, D., Bao, J., Wen, F., Zhang, B., Chen, D., Yuan, L., Guo, B.: Vector quantized diffusion model for text-to-image synthesis. In: CVPR (2022)

[21] Ho, J., Jain, A., Abbeel, P.: Denoising diffusion probabilistic models. NeurIPS (2020)

[22] Jeong, Y., Kim, D., Ro, Y., Kim, P., Choi, J.: Fingerprintnet: Synthesized fingerprints for generated image detection. In: ECCV (2022)

[23] Karras, T., Aila, T., Laine, S., Lehtinen, J.: Progressive growing of gans for improved quality, stability, and variation. ICLR (2018)

[24] Karras, T., Laine, S., Aila, T.: A style-based generator architecture for generative adversarial networks. In: CVPR (2019)

[25] Karras, T., Laine, S., Aittala, M., Hellsten, J., Lehtinen, J., Aila, T.: Analyzing and improving the image quality of stylegan. In: 2020 IEEE/CVF Conference on Computer Vision and Pattern Recognition, CVPR 2020, Seattle, WA, USA, June 13-19, 2020 (2020)

[26] Kim, G., Kwon, T., Ye, J.C.: Diffusionclip: Text-guided diffusion models for robust image manipulation. In: CVPR (2022)

[27] Kingma, D.P., Welling, M.: Auto-encoding variational bayes. ICLR14 (2013)

[28] Li, K., Zhang, T., Malik, J.: Diverse image synthesis from semantic layouts via conditional imle. In: ICCV (2019)

[29] Liu, B., Yang, F., Bi, X., Xiao, B., Li, W., Gao, X.: Detecting generated images by real images. In: ECCV (2022)

[30] Marra, F., Gragnaniello, D., Verdoliva, L., Poggi, G.: Do gans leave artificial fingerprints? In: MIPR (2019)

[31] Nichol, A., Dhariwal, P., Ramesh, A., Shyam, P., Mishkin, P., McGrew, B., Sutskever, I., Chen, M.: Glide: Towards photorealistic image generation and editing with text-guided diffusion models. ICML (2022)

[32] Ojha, U., Li, Y., Lee, Y.J.: Towards universal fake image detectors that generalize across generative models. In: CVPR (2023)

[33] Park, T., Liu, M.Y., Wang, T.C., Zhu, J.Y.: Semantic image synthesis with spatially-adaptive normalization. In: CVPR (2019)

[34] Radford, A., Kim, J.W., Hallacy, C., Ramesh, A., Goh, G., Agarwal, S., Sastry, G., Askell, A., Mishkin, P., Clark, J., et al.: Learning transferable visual models from natural language supervision. In: ICML (2021)

[35] Ramesh, A., Pavlov, M., Goh, G., Gray, S., Voss, C., Radford, A., Chen, M., Sutskever, I.: Zero-shot text-to-image generation. In: ICCV (2021)

[36] Rombach, R., Blattmann, A., Lorenz, D., Esser, P., Ommer, B.: High-resolution image synthesis with latent diffusion models. In: CVPR (2022)

[37] Rossler, A., Cozzolino, D., Verdoliva, L., Riess, C., Thies, J., Nießner, M.: Faceforensics++: Learning to detect manipulated facial images. In: ICCV (2019)

[38] Ruiz, N., Li, Y., Jampani, V., Pritch, Y., Rubinstein, M., Aberman, K.: Dreambooth: Fine tuning text-to-image diffusion models for subject-driven generation. In: CVPR (2023)

[39] Saharia, C., Chan, W., Saxena, S., Li, L., Whang, J., Denton, E.L., Ghasemipour, K., Gontijo Lopes, R., Karagol Ayan, B., Salimans, T., et al.: Photorealistic text-to-image diffusion models with deep language understanding. NeurIPS (2022)
[40] Schuhmann, C., Vencu, R., Beaumont, R., Kaczmarczyk, R., Mullis, C., Katta, A., Coombes, T., Jitsev, J., Komatsuzaki, A.: Laion-400m: Open dataset of clip-filtered 400 million image-text pairs. NeurIPS Workshop (2021)
[41] Sha, Z., Li, Z., Yu, N., Zhang, Y.: De-fake: Detection and attribution of fake images generated by text-to-image generation models. In: CCS (2023)
[42] Sohl-Dickstein, J., Weiss, E., Maheswaranathan, N., Ganguli, S.: Deep unsupervised learning using nonequilibrium thermodynamics. In: ICML. PMLR (2015)
[43] Song, Y., Sohl-Dickstein, J., Kingma, D.P., Kumar, A., Ermon, S., Poole, B.: Score-based generative modeling through stochastic differential equations. ICLR (2021)
[44] Tan, C., Zhao, Y., Wei, S., Gu, G., Wei, Y.: Learning on gradients: Generalized artifacts representation for gan-generated images detection. In: CVPR (2023)
[45] Wang, S.Y., Wang, O., Zhang, R., Owens, A., Efros, A.A.: Cnn-generated images are surprisingly easy to spot... for now. In: CVPR (2020)
[46] Wang, Z., Bao, J., Zhou, W., Wang, W., Hu, H., Chen, H., Li, H.: Dire for diffusion-generated image detection. In: ICCV (2023)
[47] Yang, Y., Wang, R., Qian, Z., Zhu, Y., Wu, Y.: Diffusion in diffusion: Cyclic one-way diffusion for text-vision-conditioned generation. ICLR (2024)
[48] Yu, F., Seff, A., Zhang, Y., Song, S., Funkhouser, T., Xiao, J.: Lsun: Construction of a large-scale image dataset using deep learning with humans in the loop. Arxiv (2015)
[49] Zhang, L., Rao, A., Agrawala, M.: Adding conditional control to text-to-image diffusion models. In: ICCV (2023)
[50] Zhang, X., Karaman, S., Chang, S.F.: Detecting and simulating artifacts in gan fake images. In: WIFS (2019)
[51] Zhu, J.Y., Park, T., Isola, P., Efros, A.A.: Unpaired image-to-image translation using cycle-consistent adversarial networks. In: ICCV (2017)
[52] Zhu, M., Chen, H., Yan, Q., Huang, X., Lin, G., Li, W., Tu, Z., Hu, H., Hu, J., Wang, Y.: Genimage: A million-scale benchmark for detecting ai-generated image. NeurIPS (2024)
[53] Zhu, Y., Wu, Y., Deng, Z., Russakovsky, O., Yan, Y.: Boundary guided learning-free semantic control with diffusion models. NeurIPS (2024)

In this appendix, we add some experiments to delve deeper into the robustness of the differentiated features. We conduct a sensitivity analysis on the only variable of the patch-shuffle operation, the patch size, in Appendix A; we use different classification heads to demonstrate the robustness of the differentiated features to the classification heads in Appendix B; we showcase the samples that were correctly identified additionally by using differentiated features compared to the baseline UFD in Appendix C; finally, we detailly report the test results of our method and the baseline across various generators in Appendix D.

A Sensitivity of Discrepancy Features to Patch Size

Table 4: Results of different patch sizes on the validation set. The ablated patch sizes range from 14 to 224 (the image size). The significant improvement brought by the switch from 224 to 112 shows the effectiveness of introducing discrepancy. Patch sizes 14, 28, and 56 achieve similarly high performance. But patch size 1's performance drops for the over-destruction of local artifacts.

Patch size	Validataion					
	In-domain		Out-of-domain		Total	
	Mean acc.	AP	Mean acc.	AP	Mean acc.	AP
1	0.958	0.992	0.837	0.934	0.885	0.960
14	0.967	0.995	0.859	0.944	0.904	0.968
28	0.966	0.995	0.871	0.939	0.909	0.965
56	0.962	0.998	0.871	0.943	0.907	0.965
112	0.949	0.989	0.858	0.942	0.895	0.964
224	0.889	0.964	0.829	0.935	0.853	0.946

We study how the patch size affects the learning from the discrepancy features. A tradeoff exists between increasing the discrepancy between features and mining the universal local artifacts, i.e. the smaller patch size offers more discrepancy but retains fewer local artifacts useful for deepfake detection. Therefore, given the original image size of 224, we conduct validations with different patch sizes, ranging from 1 to 224, to see the changing trend. These experiments adhere to the proposed experimental setting, with the patch size being the only variable adjusted. As shown in Tab. 4, changing the patch size from 224 to 112 brings a significant improvement of 6.0 points in ID accuracy and 2.9 points in OOD accuracy, suggesting that introducing additional discrepancy in features helps in expanding the representation of features and extracting universal artifacts.

The patch sizes 14, 28, and 56 yield similarly high overall performance, showing the robustness of introducing discrepancy in different patch sizes. It is worth noting that when the patch size is 1, the local artifacts of the patch-shuffled image are significantly affected, resulting in a drop in model performance compared to patch size 14. In our state-of-the-art version, we directly opt for a patch size of 14 to align with the backbone CLIP:ViT-L/14 [34] while introducing the highest discrepancy in features.

B Different Classifier Heads

We investigate how different classifier heads influence the model's performance to verify the effectiveness of artifact invariance learning. We evaluate four architectures: (i) **FC**: a single fully connected layer, (ii) **MLP**: A two-layer nonlinear perceptron network with ReLU activation and a hidden layer dimension of 2×1024 neurons, (iii) **Self-Attention**: a network consisting of a self-attention layer [14] and a single fully connected layer, and (iv) **Transformer**: A network

composed of two transformer encoder layers with 4 attention heads and a forward dimension of 4×1024 [14] and one fully connected layer.

Tab. 5 presents the results of these variants in our proposed experimental setting. The findings show that the results of MLP, Self-Attention, and Transformer are significantly improved compared to FC. This means establishing the correlations between the two discrepancy features helps learn universal artifacts. In addition, the performances of Self-Attention, MLP, and Transformer don't show an obvious gap, which demonstrates that our discrepancy features are highly distinguishable for deepfake detection.

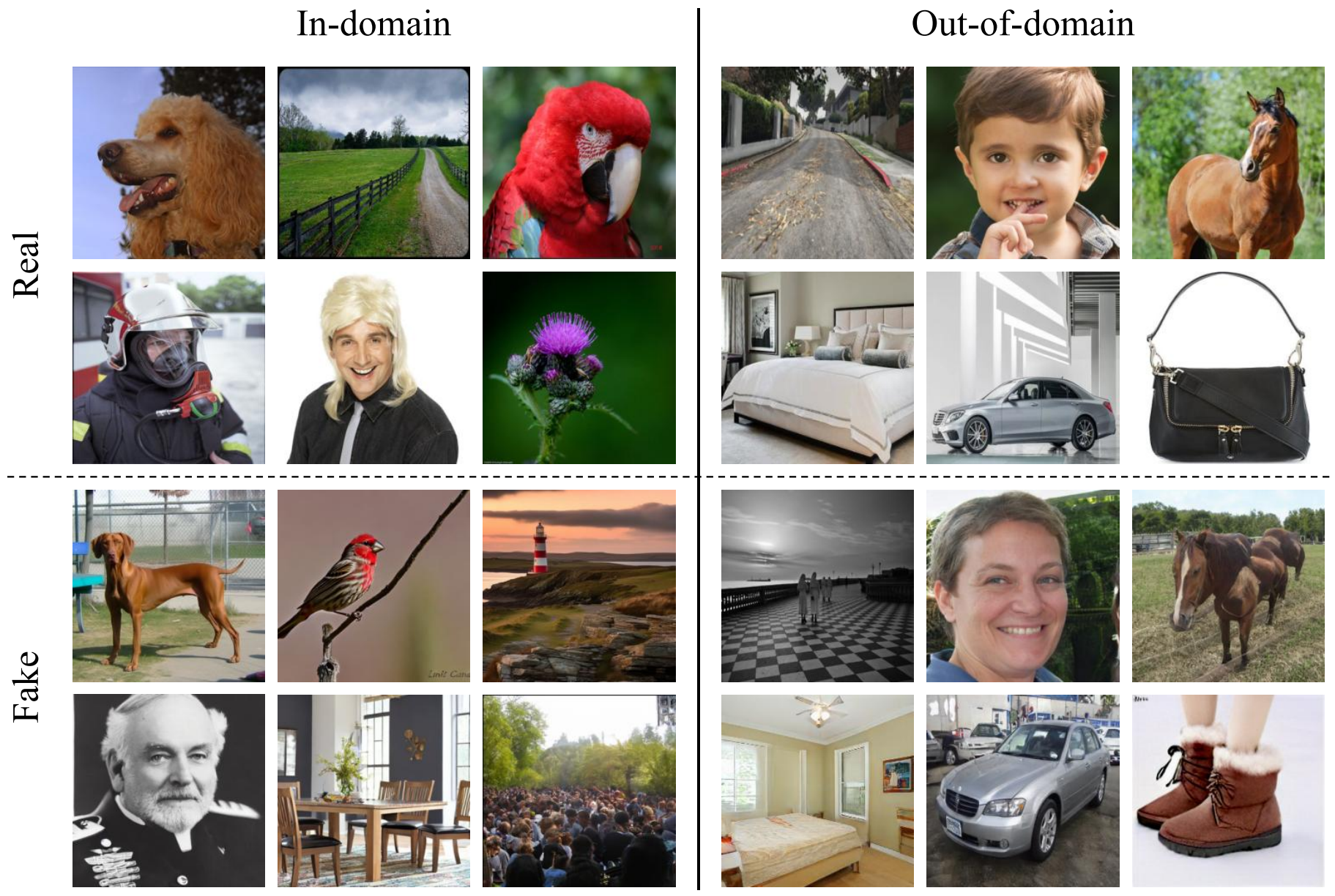

Fig. 4: Visualization of uniquely detected samples. We present a selection of samples from both in-domain and out-of-domain, that are accurately classified by our approach, yet erroneously classified by the UFD [32], with a discrepancy in classification confidence exceeding 0.8.

C Comparative Analysis of Uniquely Detected Samples

We take a further step to explore how our method outperforms. We present a selection of samples from both in-domain and out-of-domain. These samples are accurately classified by our approach, yet erroneously classified by the UFD [32], with a discrepancy in classification confidence exceeding 0.8. As shown in Fig.4, these samples are challenging to discern with the naked eye. This compellingly demonstrates that our method is capable of learning deeper and more universal artifacts, thereby retaining its effectiveness even when confronted with such challenging samples.

D Detailed Mean Accuracy Results of Comparisons with the State-of-the-arts

In this section, we report the detailed mean accuracy results of comparisons with the state-of-the-art in Tab. 6, as a supplement to Table 1 in Sec 4.5, including ADM [13], BigGAN [4], GLIDE [31], Midjourney [2], LDM [36], VQDM [20], wukong [3], ProGAN [23], CycleGAN [51], StyleGAN [24], StyleGAN2 [25], GauGAN [33], StarGAN [8], Deepfakes [37], whichfaceisreal [1], SITD [6], SAN [11], CRN [7], IMLE [28], and DALL·E [35]. Results of generators with the same architecture but different parameters are averaged. For example, the result of BigGAN [4] in this table is the average of BigGAN in UFD [32] and BigGAN in GenImage [52].

Table 5: Results of different classifier heads on the validation set. We evaluate four classifier network architectures and find that a network that learns the correlations between features will perform better.

Architecture	Validataion					
	In-domain		Out-of-domain		Total	
	Mean acc.	AP	Mean acc.	AP	Mean acc.	AP
FC	0.918	0.977	0.835	0.938	0.868	0.954
MLP	0.960	0.995	0.865	0.932	0.903	0.963
Self-Attention	0.967	0.995	0.859	0.944	0.904	0.968
Transformer	0.965	0.995	0.872	0.952	0.909	0.973

Table 6: Detailed mean accuracy results of comparisons with the state-of-the-art on the testing set. We report the mean accuracy per generator in the percentage form. Results of generators with the same architecture but different parameters are averaged.

methods	In-domain								Out-of-domain														
	ADM	BigGAN	GLIDE	Midjourney	LDM	VQDM	wukong	ProGAN	CycleGAN	StyleGAN	StyleGAN2	GauGAN	StarGAN	Deepfakes	which-faceisreal	SITD	SAN	CRN	IMLE	DAL·LE	ID	OOD	Total
CNNDet	89.6	79.1	98.2	97.3	93.7	97.0	95.7	95.6	72.0	75.7	80.0	56.4	98.2	80.2	47.3	49.7	72.4	56.0	56.0	94.7	93.3	69.9	79.2
Patchfor	99.8	85.1	99.6	99.6	99.7	99.7	99.7	99.9	93.2	98.1	94.4	59.1	99.8	90.7	61.6	65.4	84.5	50.0	50.0	99.6	97.9	78.9	86.5
LNP	91.0	72.5	95.0	94.4	92.2	89.4	92.8	87.3	71.0	89.9	85.0	68.8	83.7	65.5	53.9	52.0	55.8	50.1	62.6	84.6	89.3	68.6	76.9
DIRE	99.9	82.6	99.9	99.8	99.9	100	100	98.4	60.3	94.2	95.1	55.3	88.6	67.9	50.0	50.0	59.7	50.0	50.0	99.7	97.6	68.4	80.1
UFD	83.2	92.0	86.3	80.2	85.4	89.0	85.6	91.1	74.8	79.4	82.4	95.5	89.0	75.9	79.8	73.1	61.9	87.9	90.0	86.6	86.6	81.4	83.5
Ours	94.8	98.5	95.0	96.8	94.4	96.7	97.1	99.4	92.7	94.9	95.7	98.1	96.0	67.7	83.1	73.8	62.6	88.1	95.0	92.8	96.6	87.6	90.7